Eddy-resolving modeling of overflows

S. Legg

NOAA-GFDL, Princeton University Forrestal Campus, 201 Forrestal Rd,

Princeton, NJ 08540, USA.

L. Jackson

NOAA-GFDL, Princeton University Forrestal Campus, 201 Forrestal Rd,

Princeton, NJ 08540, USA.

R.W. Hallberg

NOAA-GFDL, Princeton University Forrestal Campus, 201 Forrestal Rd,

Princeton, NJ 08540, USA.

S.Legg, NOAA-GFDL, Princeton University Forrestal Campus, 201 Forrestal Rd, Princeton, NJ 08540. Sonya.Legg@noaa.gov

Abstract. Dense waters flowing through narrow topographic constrictions or down sloping topography as dense overflows are responsible for generating most of the deep water masses of the ocean, following mixing with overlying waters. Overflows involve a variety of different physical processes which together determine the volume, transport and tracer properties of the dense water mass when it reaches the open ocean. Here we review the current state of eddy-resolving modeling of overflows, and understanding of mesoscale eddy processes active in overflows, focusing on models where mesoscale eddies are resolved, but small-scale mixing is not. At these resolutions, the significant remaining difficulty is the treatment of diapycnal mixing, and we examine the dependence of this mixing on model parameterizations and numerics in overflow simulations.

1. Introduction

Dense water, formed in marginal seas or on continental shelves, enters the large scale ocean circulation in the form of overflows or gravity currents, often flowing through narrow straits and down topographic slopes. Climatologically important overflows include the dense flows through the Denmark Straits, the Faroe Bank Channel, the Gibraltar Straits, and from Red Sea and the Antarctic shelves. The water masses originating in these overflows (e.g. North Atlantic Deep Water, Mediterranean Sea Water and Antarctic Bottom Water) fill much of the deep ocean. Many different physical processes may be important in controlling the transport of dense water through overflows and its mixing with the ambient water. These include processes such as hydraulic control at sills and straits [*Girton et al.*, 2006], [*Kase and Oschlies*, 2000], hydraulic jumps downstream of topographic constrictions [*Holland et al.*, 2002], interactions with narrow canyons, mesoscale eddies generated through instability of the overflow plume [*Bruce*, 1995], [*Geyer et al.*, 2006], [*Serra and Ambar*, 2002], interactions with overlying water masses and interactions with tidally-driven currents [*Gordon et al.*, 2004]. Other processes are associated with small-scale diapycnal mixing, e.g. shear-driven mixing in the rapid down-slope flows [*Mauritzen et al.*, 2005], [*Price et al.*, 1993], [*Peters et al.*, 2005], bottom friction [*Peters and Johns*, 2006], and diapycnal mixing associated with internal waves and internal tides. While most of these processes are not captured by large-scale climate models, which may not even resolve the scale of the channel from which the overflow originates, mesoscale-eddy resolving models are able to explicitly simulate many of these processes. The exceptions are those associated with small-scale diapycnal mixing. The major challenge therefore for

simulations of overflows at eddy-resolving resolution (i.e. high enough to resolve mesoscale eddies) is in the correct representation of the small-scale diapycnal mixing.

In this chapter we will outline the current status of mesoscale-eddy-resolving modeling of overflows, review the understanding of some of the above physical processes obtained by previous eddy-resolving simulations of overflows, and discuss the difficulties that remain, particularly in correctly representing the diapycnal mixing processes in eddy-resolving simulations, where diapycnal mixing may be both explicitly parameterized and result from numerical advection schemes.

2. Previous eddy-resolving studies of overflows

Eddy-resolving simulations of overflows are relatively recent and few in number. Since overflows by definition occur in regions of steep topographic slope, may have small widths/thicknesses, and are often associated with small deformation radii, as well as strong localized mixing, it is only recently that models have been able to simultaneously cope with all these constraints within realistic regional ocean configurations.

Much of our understanding of the processes acting in overflows therefore comes from idealized simulations and laboratory experiments which allow examination of the sensitivity of mixing to various parameters under controlled conditions. Many of these idealized simulations have represented the overflow as a dense inflow forced through a narrow channel onto a uniform slope, beginning with *Jiang and Garwood* [1996], and continuing with the Dynamics of Overflow Mixing and Entrainment (DOME) collaboration [*Ezer and Mellor*, 2004],[*Ezer*, 2005], [*Legg et al.*, 2006]. In these simulations, provided resolution is sufficiently high, the dense plume proceeds diagonally down the slope with the path determined by a balance between the Coriolis forces and frictional forces. A large number

of eddies often develop on the downslope side and entrain ambient fluid into the plume, altering its characteristics. Both frictional processes and the eddies appear to be important in controlling the downslope flow of the dense fluid. Similar eddy formation has been seen in laboratory experiments [*Lane-Serff and Baines*, 1998],[*Cenedese et al.*, 2004], and in observations downstream of the Denmark Straits [*Bruce*, 1995] and Faroe Bank Channel [*Geyer et al.*, 2006]. From these simulations and laboratory experiments, as well as theoretical work, an understanding of the scales and regimes present in overflows has been obtained and is summarized here. Obviously these idealized simulations and laboratory experiments examine only a few of the overflow processes in isolation, in order to reduce the complexity of the problem. In particular, the DOME scenario focuses on the mesoscale eddies generated through instabilities of the overflow plume, and includes both bottom friction and shear-driven mixing, but omits most other important physical processes. Nonetheless it is a useful starting point for understanding overflows where eddying behavior is observed (e.g. the Denmark Straits, Faroe Bank Channel and Gibraltar Straits overflows).

2.1. Processes, scales and regimes in rotating overflows

In the absence of friction, a geostrophically balanced dense current would flow along isobaths with a velocity

$$U_N = \frac{\alpha g'}{f}, \tag{1}$$

a velocity scale known as the Nof speed [*Nof*, 1983], where g' is the buoyancy anomaly of the overflow plume, α is the slope of the topography and f is the Coriolis parameter.

Frictional processes allow flow to cross isobaths so that the angle of the frictionally-driven downslope flow is predicted by

$$tan(\theta) \sim \frac{C_d U_N}{f h_0} = \text{ drag Ekman number} \tag{2}$$

when quadratic bottom drag is the dominant source of friction. Here C_d is the bottom drag and h_0 is the depth of the overflow layer [*Price and Baringer*, 1994]. *Killworth* [2001] proposes a model for the dense plume in which h_0 is prescribed in terms of g' and U from a Froude number criterion (assuming turbulent bottom boundary layer processes are responsible for determining the depth h_0), which leads to a prediction that the rate of vertical descent ($\alpha tan(\theta) = dD/dl$, where D is the vertical location of the plume and l is the along-plume distance) should be a constant for all overflows (presuming the same turbulent processes apply in all cases).

For linear bottom drag the angle of descent is:

$$tan(\theta) \sim R_u/f. \tag{3}$$

[*Kida*, 2006], where R_u is the linear drag coefficient (with units of s^{-1}). These estimates for the downslope flow angle ignore mixing (which can modify g') and eddies (which provide a further mechanism for downslope transport) and assume the overflow layer is homogeneous, so that the bottom drag is applied over the whole dense layer.

If instead of bottom drag, we have Laplacian friction, vertical gradients in velocity in the dense layer will of course be important. However, from simple dimensional arguments we might predict the angle of descent to again follow an Ekman number-type scaling:

$$tan(\theta) \sim \frac{\nu_z}{f h_0^2} \sim \text{ frictional Ekman number} \tag{4}$$

where ν_z is the vertical viscosity.

There has been considerable discussion as to the physical mechanism responsible for the eddies seen in laboratory experiments, numerical simulations and the ocean. *Swaters* [1991] has shown analytically that a lens of dense water on a slope may be unstable to a form of baroclinic instability, leading to eddy formation on the downslope side of the dense current. The instability theory predicts that these eddies will be anticyclonic in the dense layer of the fluid, with cyclonic vortices in the upper layer. In this theory the instability growth rate is predicted to scale with the parameter

$$\mu = \frac{h_0}{\alpha L_{\rho D}} = \frac{h_0 f}{\alpha \sqrt{g' D}}, \tag{5}$$

where $L_{\rho D} = \sqrt{g' D}/f$ is a deformation radius based on the depth of the fluid layer (assumed to be unstratified) above the plume, D.

In contrast *Lane-Serff and Baines* [1998] (hereafter referred to as LSB98) focus on the vorticity changes induced in the fluid above the overflow. They suggest that the eddies are produced as a result of increased cyclonic vorticity in this layer through potential vorticity (PV) conservation when fluid which is initially high on the slope (i.e with high absolute PV) is moved to a position lower on the slope (where ambient PV is lower). This instability is therefore a barotropic instability resulting from the generation of a local extremum in potential vorticity by the advection of fluid down the slope. The mechanisms proposed for moving the upper layer fluid downslope include a coupling with the dense underlying fluid, geostrophic adjustment of the lower layer, and draining of the lower layer by viscous processes. They argue that the eddies are barotropic and cyclonic. LSB98 propose that the relevant parameter to describe this stretching of the upper water column is the parameter

$$\Gamma = \frac{L_{\rho h_0} \alpha}{D} = \frac{\sqrt{g' h_0} \alpha}{f D} \tag{6}$$

where $L_{\rho h_0} = \sqrt{g'h_0}/f$ is the deformation radius based on the thickness of the overflow layer. LSB98 find that both the strength of the eddies and their frequency increased as Γ increased. They only observed eddies when $\Gamma > 0.05$, perhaps because otherwise the timescale required for eddies to evolve is too long to be observed. However, it should be noted that they only examined $\Gamma < 0.5$, and one might expect a very different regime, with no eddies, for small f, i.e. large Γ. We can estimate the boundary for the eddy dominated regime by considering that the overflow becomes geostrophically adjusted after a distance of about $L_{\rho h_0}$. Then the vertical distance moved down the slope is $\alpha L_{\rho h_0}$. Now if this vertical distance is greater than the total depth of the fluid, geostrophic adjustment would not occur while the dense overflow is on the slope, and the plume would therefore not be rotationally constrained. So a plume is not rotationally constrained if

$$\alpha L_{\rho h_0} > D \rightarrow \frac{\alpha\sqrt{g'h_0}}{Df} = \Gamma > 1 \tag{7}$$

Cenedese et al. [2004] indeed find that eddies are not generated for low f.

To compare the baroclinic instability and vortex stretching arguments for eddy formation, one should note that the two key parameters are in fact closely related:

$$\mu = \frac{1}{\Gamma}\left(\frac{h_0}{D}\right)^{3/2} \tag{8}$$

and they are both related to a further parameter

$$M = \alpha/S = \frac{\alpha}{f}\sqrt{g'/h_0} = \Gamma\frac{D}{h_0} = \frac{1}{\mu}\left(\frac{h_0}{D}\right)^{1/2} \tag{9}$$

where S is the "geostrophic slope", i.e. the ratio $h_0/L_{\rho h_0}$. However, LSB98 find that their data collapse against Γ, but not against μ or M. Nonetheless, recent experiments by *Decamp and Sommeria* [2007] indicate that when D is constant, results do scale with M. The sign of vorticity expected in the eddies in the dense layer is opposite in the two

scenarios. *Etling et al.* [2000] suggest from their laboratory experiments that the upper layer cyclone generation dominates if μ is small, while baroclinic instability dominates if μ is large.

Careful studies with adiabatic (i.e. isopycnal models) have helped to show that both mechanisms may be possible in overflow scenarios. *Kida* [2006] demonstrates instability in a dense current which is already geostrophically balanced as it exits the channel flowing almost along topographic contours. The tendency for upper layer fluid to be drawn down the slope by coupling with the lower layer fluid is therefore limited, and generation of cyclonic vorticity through stretching is small. Because a layered model is used, the dense layer does not lose fluid downslope through viscous draining, instead the whole layer moves downslope. The dense current becomes unstable and breaks up into a series of anticyclonic eddies. The motion in the upper layer consists of alternating cyclones and anticyclones. The instability growth rate and length-scale appear to be well predicted by Swaters' instability theory. In particular, as predicted in Swaters' theory, the growth-rate is greatly diminished if D, the depth of the upper layer fluid, is increased. No tendency for cyclone generation is found even at small μ, unlike the results seen in the laboratory experiments of *Etling et al.* [2000] and LSB98. This suggests that a key difference could be the mechanism for generating the dense current - initializing it moving along slope in geostrophic adjustment - in this study.

Alternatively, *Spall and Price* [1998] (hereafter SP98) show that when the flow exiting the strait has a strong barotropic component, including a component at intermediate densities, this intermediate fluid layer is indeed stretched as the dense current descends the slope. A barotropic instability results in which cyclonic eddies, with maximum amplitude

above the dense layer, are generated. This scenario seems to fit the LSB98 model, although the vortex stretching in the intermediate layer is enhanced because of the net flow in that layer. SP98 show that without the flow in the intermediate layer a weaker instability results - they examine how the coupling between the layers generates a flow from shallow to deep regions in this layer and hence generates cyclonic vorticity, although more weakly than the LSB98 mechanism. The scenario with barotropic flow is especially pertinent to the Denmark Straits overflow, where the flow through the strait includes an Artic Intermediate Water layer, in addition to the densest deep water. SP98 suggest that this is a reason for more active upper ocean eddies in the Denmark Straits overflow region compared to other overflows.

All the above experiments/simulations have been for an ambient fluid which is either unstratified or consists of a few layers. *Lane-Serff and Baines* [2000] (hereafter LSB2000) examine the scenario of a dense overflow entering a region of stable stratification. Now the vertical coupling between overflow and overlying fluid is limited by stratification to a height

$$d_N = L_{\rho h_0} f/N, \tag{10}$$

so that the stretching parameter for a stratified fluid becomes

$$\Gamma_N = \frac{L_{\rho h_0}\alpha}{d_N} = \frac{N\alpha}{f} \tag{11}$$

which, interestingly, is independent of the buoyancy anomaly and depth of the dense current itself. According to LSB2000, stratification is only expected to significantly affect the evolution of eddies if $d_N < D$, or equivalently $\Gamma_N > \Gamma$. Their laboratory experiments for the stratified case again only find a regime of eddies for $\Gamma_N > 0.05$, but once again only $\Gamma_N < 0.5$ was considered. According to LSB2000, if stratification is important, its effect is

always to enhance the barotropic instability, because the relative PV gradients in a layer of thickness d_N are greater than those in a layer of thickness D when $d_N < D$. However it can also be argued that stratification may suppress the downslope displacement of the overlying fluid (energetically, downslope displacement cannot exceed U/N where U is the velocity scale of the motion). Then, in the presence of strong stratification, the dense overflow layer could become uncoupled from the fluid above it if the dense water descends much further down the slope than a distance d_N. LSB2000 do not consider what is perhaps the most important effect of stratification on the overflow - that the overflow water will not necessarily penetrate all the way down the slope, but will rather detrain when the plume reaches its neutral buoyancy level (as shown by *Jiang and Garwood* [1998] and the DOME simulations [*Ezer*, 2005; *Legg et al.*, 2006]). If the neutral buoyancy level were reached before eddy formation occurred, a very different regime might be observed. This regime transition would occur when the depth of the neutral buoyancy level is less than the vertical distance over which geostrophic adjustment occurs, i.e. when

$$\frac{g'}{N^2} < \alpha L_{\rho h_0} \rightarrow \frac{1}{r} < \Gamma_N \tag{12}$$

where r is the "relative stratification" $r = N/\sqrt{g'/h_0}$, the ratio of plume stratification to ambient stratification, described by LSB2000. When $r\Gamma_N > 1$ the overflow plume will reach its neutral buoyancy level and detrain into the fluid interior before eddy processes have a chance to develop. (Note LSB2000 only considered $r\Gamma_N < 1$).

When eddy processes do develop before the neutral buoyancy level is reached, the eddies appear to play a significant role in this detrainment process, enabling interleaving of plume fluid with ambient fluid at the same density in the ocean interior [*Jiang and Garwood*, 1998; *Legg et al.*, 2006].

Cenedese et al. [2004] and *Smith* [1977] have found that the eddy regime only exists for small Ekman numbers, i.e. $Ek = 2\nu/(fh_0^2) < 0.1$ (and Froude numbers less than unity). For larger Ek, the flow is found to be laminar. SP98 similarly find that large bottom drag prevents the formation of eddies, and they suggest that larger bottom drag/friction causes the overflow layer to descend so rapidly that it decouples from the overlying fluid, and hence preventing the formation of eddies by the vortex stretching mechanism.

The length-scale L of the eddies appears to depend on the mechanism responsible for creating them. *Kida* [2006] finds that when baroclinic instability is responsible for creating the eddies, the length-scales are well predicted by the wavelength of the fastest growing mode, which in turn is of the order of $L_{\rho D}$, in unstratified ambient fluid. LSB98 find that the length scale of eddies in the vortex-stretching regime is close to $L_{\rho h_0}$. SP98 by contrast find an eddy length scale that appears to be independent of f. They find this length scale is well predicted by assuming that the volume of fluid contained within an eddy divided by the eddy generation timescale has to equal the imposed outflow transport, so that

$$\frac{\pi L^2 h_0}{T_e} = Q \rightarrow L = \left(\frac{2Q}{\alpha N h_0}\right)^{1/2} \tag{13}$$

where Q is the outflow transport. $T_e = \frac{2\pi}{\alpha N}$, is the eddy generation time, where the eddy frequency is $\omega = -\alpha N$, as for a short topographic Rossby wave. For SP98, N is determined from the layer model by the density difference between the layers.

LSB98 have a similar estimate for an eddy generation timescale which appears to scale like $T_e \sim 1/(f\Gamma)$. Their explanation for this timescale is different however: if the eddies move at the Nof speed $u_N \sim g'\alpha/f$ (as is seen to some extent in the experiments), and

have a radius $L \sim \sqrt{g'h_0}/f$, then the minimum time between eddies must be

$$T_e \sim \frac{2L}{u_N} \sim \frac{1}{\alpha}\sqrt{\frac{h_0}{g'}}. \tag{14}$$

However, these length, time and velocity scales do not lead to a total transport which matches the imposed outflow transport, implying that there is some missing physics not accounted for in these scaling arguments.

For a stratified flow, LSB2000 suggest that eddy radii should again scale like $L_{\rho h_0}$. There is a suggestion from comparison of DOME calculations with and without stratification, that the eddy radius is reduced by the introduction of stratification [*Legg et al.*, 2006], but whether this can be explained by the change in g' due to the stratification has not been verified quantitatively. (Changes in g' leading to changes in eddy radius can also be introduced by changes in mixing due to sill topography and slope, [*Ezer*, 2006].)

None of these arguments for eddy scales and regimes takes into account diapycnal mixing. Mixing appears to be most sensitive to the Froude number

$$Fr = U/\sqrt{g'h_0} \tag{15}$$

or, equivalently, the Richardson number $Ri = 1/Fr^2$, where U is the velocity of the gravity current relative to the environment. This is seen in numerous studies of nonrotating gravity currents [*Ellison and Turner*, 1959; *Özgökmen and Chassignet*, 2002] where mixing is found only when $Fr > 1$. *Cenedese et al.* [2004] find that the Froude number also separates eddying regimes from non-eddying regimes: specifically they only found eddies for $Fr < 1$, and when $Fr > 1$ they found a different, wave-dominated regime, even with strong rotation. However, these laboratory experiments were at relatively low Reynolds numbers, and it is not certain whether the wave-dominated regime would persist at high

Re, or transition to a more turbulent flow. *Ezer* [2006] finds a similar supercritical, wave-like regime when $Fr > 1$ in numerical simulations. It should be noted that a single overflow may transition from a $Fr > 1$ regime, to a $Fr < 1$ regime via a hydraulic jump, and one would expect most of the mixing to occur in the supercritical regime, and most of the eddy behavior to occur in the subcritical regime.

In summary, several parameters determine the behavior of eddies and mixing in overflows: the Ekman number (high values leading to laminar overflows), the Froude number (high values leading to mixing), and some form of a stretching parameter Γ, with values of $\Gamma < 1$ leading to eddies. Eddies may be generated by barotropic or baroclinic instability, with the nature of the overflow (the extent to which it is initially ageostrophic and/or barotropic) determining the relative importance of each. Some questions remain concerning the transitions between barotropic and baroclinic instability and the dominant length and timescales, particularly for overflows in stratified ambient flow.

2.2. Realistic eddy-resolving simulations of overflows

While these idealized simulations and laboratory experiments have done much to identify the processes active in dense overflows (namely baroclinic instability, vortex stretching and frictional drainage) real overflows are obviously much more complicated than represented in these idealized geometries, and include many more active physical processes. Realistic eddy-resolving simulations of overflows are relatively recent due to the high resolution required. Estimates of the lengthscales of eddies can be made from the scaling arguments given above: For the Denmark Straits, LSB98 predict an eddy length-scale of about 18km and SP98 find eddies of about 30km in diameter for Denmark Straits parameters. Other overflows with smaller g' and or h_0 will have smaller horizontal lengthscales.

Hence in order to resolve eddies and narrow topography, horizontal resolutions of less than 5km are necessary. The specification of boundary conditions for the limited area simulations, involving inflows and evolving outflows, can be difficult. Many simulations have used a "dam break" initialization/forcing, whereby the dense water is initially contained entirely within an upstream basin; a dam at the strait or sill is removed instantaneously, and the overflow is allowed to evolve until such time as the downstream boundary conditions begin to influence the solutions. Despite the fact that these simulations are far from the continuous overflows found in nature, the quasi-steady state usually achieved downstream of the sill often has many similarities with the real overflows.

An example of such a dam-break simulation is the Denmark Straits overflow simulation performed by *Käse et al.* [2003], using a 4km resolution terrain-following model. This simulation shows many of the features noted by SP98 in their more idealized model, namely generation of barotropic eddies due to vortex stretching at the location where the dense flow begins its descent down the slope. They note however that further downstream the flow is more baroclinic, and baroclinic instability may be more important there. In this downstream regime the flow has become geostrophically balanced and is moving along the slope as in the idealized study of *Kida* [2006]. Perhaps as suggested earlier, the ambient stratification limits the extent over which the vortex stretching mechanism can operate, and a geostrophic, purely density-driven current, appears to be more likely to lead to baroclinic instability. While the eddy behavior appears to agree well with observations, the model entrainment (resulting from diffusion, convective adjustment and the advection scheme) occurs earlier than seen in observations. More recently (Tom Haine, private communication) 2km resolution simulations of the Denmark Straits overflow region

using the MITgcm with more complex inflow and outflow boundary forcing demonstrate a further likely role for the eddies generated in the surface layer as a result of the overflow: the surface circulation of these eddies seems to entrain cold water from the Greenland Shelf, intermittently flushing it into the open ocean.

The Mediterranean overflow has been simulated at high resolution by several authors [*Jungclaus and Mellor*, 2000; *Papadakis et al.*, 2003; *Xu et al.*, 2007]. *Jungclaus and Mellor* [2000] carry out simulations of the Mediterranean outflow at 5km resolution using the terrain-following coordinate Princeton Ocean Model. They find instability in the Gulf of Cadiz which generates eddies on a scale of about 100km. These eddies are injected into the interior at their neutral buoyancy level and appear similar to the observed "Meddies". The simulated outflow is found to have a double core structure, similar to the observations, which results from the vertical structure in the initial outflow shielding the lower portion of the overflow from mixing, and from channeling of the deepest part of the overflow down the slope by a steep canyon.

Papadakis et al. [2003] also find Meddy-like eddy generation in their simulations with the Miami Isopycnic model at 1/12 deg resolution. Their focus is on the dependence of the overflow to the subgridscale mixing parameterization: without explicitly parameterized mixing, the dense overflow in this isopycnal model was able to descend to the bottom of the Atlantic, while with the mixing parameterization more realistic entrainment was found, with the plume reaching a neutral buoyancy level. More recently the Mediterranean outflow has been used as a testbed for new entrainment parameterizations [*Xu et al.*, 2007]. *Kida et al.* [2007] has demonstrated, using highly idealized two-layer simulations, but with the Mediterranean topography, that the overflow and its eddies, through interaction with

the topographic slope, can lead to the generation of a topographic beta-plume which may extend across the ocean basin and may be a model for the Azores Current. The magnitude of this current is predicted to be highly sensitive to the amount of entrainment, and to the interaction of eddies with the topography.

The Faroe Bank Channel forms the second major source of deep water in the North Atlantic (after the Denmark Straits). While the channel itself is very narrow, about 100km downstream of the channel the dense flow spreads out onto a broad slope. Eddy-like oscillations in transport have been observed [*Geyer et al.*, 2006], as in the Denmark Straits, but unlike the Denmark Straits there is no barotropic flow through the channel since the channel only constrains the deepest and densest waters. Recent simulations of this overflow using the MITgcm at 2km resolution [*Riemenschneider and Legg*, 2007] find that most of the entrainment occurs about 50-100km downstream of the source, at around the location where the dense plume suddenly widens. Ongoing research suggests this may be a location of a lateral hydraulic jump [*Pratt et al.*, 2007]. The magnitude and location of entrainment are similar to that seen in observations [*Mauritzen et al.*, 2005], but the simulated overflow plume is slightly more diffuse. Downstream of the widening, eddy activity is found. Similar transitions between a supercritical regime downstream of the sill, and a eddy-dominated subcritical regime further downstream are found by *Ezer* [2006], using a much more idealized topography in the terrain-following coordinate Princeton Ocean Model at 2.5km resolution. As in the laboratory experiments of *Cenedese et al.* [2004] the transition between the supercritical regime and the subcritical eddying regime was found to depend on the Froude number of the flow.

Simulations of the Red Sea overflow have been carried out by *Chang et al.* [2007] using the Hybrid Coordinate Ocean Model (HYCOM), including parameterization of entrainment. The Red Sea overflow proceeds through two very narrow channels which play an important role in shielding the densest water from mixing. Due to the combination of the low latitude and narrow channel width, the channels are much smaller than the deformation radius, so that rotation plays a minimal role. Simulations showed that whereas at a resolution of 0.5km the overflow structure was well represented compared to observations, at 5km resolution the topography could not be resolved, and hence the overflow evolution was poorly represented.

2.3. The role of eddies and diapycnal mixing in overflows

Unlike mesoscale eddy-resolving simulations of, for example, the Gulf Stream, high resolution simulations of overflows, while they capture eddy processes, still do not explicitly simulate what is perhaps the dominant process, the overturning and mixing. The influence of diapycnal mixing on the overflow is obvious and direct: more mixing leads to a more diluted overflow product water, and a shallower neutral buoyancy depth (in the Mediterranean, for example). The key remaining challenge for mesoscale-eddy resolving simulations of overflows is therefore the correct representation of subgridscale diapycnal mixing.

By comparison, the role of eddies is more subtle and secondary to the mixing. For example eddies enhance the rate of downslope flow. *Kida* [2006] in particular shows that the rate of descent is increased (by about factor of two) in the region where the instability is developing, compared to a case where there is no instability (due to an increase in the total depth of the fluid) and friction alone drives the descent. Even in the

eddying simulation, further downstream when the eddy activity has saturated the rate of descent reverts to the frictionally driven value given by equation 3. It is not clear how well these results translate to other scenarios (e.g. with ambient stratification) because few simulations have compared eddying and non-eddying rates of descent for the same frictional parameters.

In a stratified ambient fluid a significant role of eddies is in effecting the detrainment of the overflow fluid away from the topography once the neutral buoyancy level is reached (for example in the Mediterranean overflow). Another role of eddies is in influencing the upper ocean circulation. The upper ocean velocities due to the cyclonic eddies generated by the overflow, for example in the Denmark Straits region, may significantly influence transports and mixing between shelf water and deeper ocean (e.g. the Greenland Shelf "spill jets" seen in simulations by Tom Haine, private communication; see also *Pickart et al.* [2005]). *Kida et al.* [2007] shows that mean flows in the upper ocean are also sensitive to the overflow eddies: in particular the eddies play an important role in connecting a topographic beta plume to the open ocean in a region of steep slope, allowing a zonal jet (similar to the Azores current) to be established.

Diapycnal mixing and eddies may also influence one another in overflows: eddies certainly lead to stirring and generation of narrow filaments, which in numerical models often lead to diapycnal mixing. It is uncertain at present the degree to which such mixing is representative of true physical processes. The extent to which diapycnal mixing influences the evolution of the eddies is also uncertain, since most parameter studies have been done in isopycnal models without mixing, or laboratory experiments where the mixing cannot be easily measured.

Given the dominant role that unresolved diapycnal mixing plays in influencing the overflows in mesoscale-eddy-resolving simulations, the focus of the rest of this chapter is therefore on the uncertainties in representation of subgridscale mixing processes in these simulations.

3. Sensitivity of overflows to model closures

Although eddy-resolving calculations are able to explore the rich eddy behavior associated with overflows, and have little difficulty capturing the effects of the topography on the flow, the representation of diapycnal mixing in such simulations remains a challenge. Numerical simulations generally include two different types of diapycnal mixing. Firstly explicit diffusivities may be used, often of the Laplacian or biharmonic form, which may have constant values, or be deduced as part of a boundary-layer parameterization scheme. For example, *Ezer and Mellor* [2004] describe simulations in the DOME configuration with constant Laplacian diffusivities in the horizontal, and vertical diffusivities deduced from the Mellor-Yamada scheme. Secondly, numerical diffusivity may result from the smoothing processes inherent in many shape-preserving advection schemes. Models with isopycnal coordinates have no numerical diffusivity, and all diapycnal mixing results from the explicit parameterization only, but both terrain-following and z-coordinate models are subject to numerical diffusivity. In *Legg et al.* [2006] (hereafter LHG06) all simulations with the z-coordinate MITgcm included no explicit diffusivity, so all the (considerable) diapycnal mixing resulted from the advection scheme. The ideal model would have negligible numerical diffusion, so that all diapycnal mixing is effected by a well-controlled physical parameterization; however this is not possible for height and sigma coordinate models. We might therefore expect net diapycnal mixing to depend on the combination

of vertical coordinate, advection scheme, and explicit parameterization of diffusivity. The other important consideration for subgridscale processes is the model viscosity. Because non-isopycnal coordinate models may include both explicit and implicit diapycnal mixing, it is very important to diagnose and evaluate the total mixing, and ascertain its dependence on model numerics.

Studies to date examining the dependence of overflow representation on these factors at eddy-resolving resolution include *Ezer and Mellor* [2004],*Ezer* [2005], LHG06 and *Tseng and Dietrich* [2006]. All employ the idealized DOME configuration. Here we will briefly review the results, focusing only on those simulations at eddy-resolving resolution (i.e. $\Delta x \leq 10km$). Unfortunately there is no "truth" against which to compare the mixing in these simulations; although several laboratory experiments have been carried out in a similar set-up to the DOME scenario [*Cenedese et al.*, 2004; *Lane-Serff and Baines*, 1998, 2000; *Etling et al.*, 2000; *Decamp and Sommeria*, 2007], only *Cenedese et al.* [2004] directly measured the entrainment, and then only in a low Re regime. Furthermore, whereas most of the numerical simulations have been carried out for a regime with ambient stratification, most of the laboratory experiments are for an unstratified ambient fluid. Similarly, many large eddy simulations and direct numerical simulations of non-rotating gravity currents exist, but none in this rotating regime. One reason is the enormous resolution necessary to resolve the range of scales which encompasses the mesoscale eddies and the overturning eddies responsible for small-scale mixing. A recommendation for future work therefore would be to carry out detailed measurements of mixing in high Reynolds number, strongly rotating gravity currents in a stratified ambient fluid. However, while we do not have a "truth" against which to compare, it is nonetheless useful to carry

out an examination of the sensitivity of model diapycnal mixing to model parameters, as follows.

Ezer and Mellor [2004] compared sigma-grid and z-level grid simulations using a generalized coordinate model [*Mellor et al.*] that used the same numerics for both grids, the same vertical viscosity and diffusivity (Mellor-Yamada scheme) [*Mellor and Yamada*, 1982], but various values of constant Laplacian diffusion and viscosity. The horizontal diffusivity and viscosity maintain a constant ratio of 1:5, and the diffusivity values vary from $10 - 10^3 m^2/s$. As would be expected, increasing the diffusion and viscosity in the along-sigma direction leads to a suppression of the eddies in the sigma-coordinate simulations. The z-coordinate simulations perform poorly in terms of moving fluid down the slope, possibly attributable to the excessive mixing generated by the Mellor-Yamada scheme when combined with the stair-step topography, or because the lateral diffusion which is applied in the horizontal direction in the z-coordinate model includes a strong diapycnal component. Both vertical coordinate models used a MPDATA advection scheme, which according to the authors necessitates non-negligible explicit diffusivity in the z-coordinate implementation. Despite the relatively poor performance of the stepped topography z-level grid with respect to down-slope plume penetration, increasing the horizontal and vertical resolution in the z-level model converged the results toward the results of the lower resolution sigma grid.

LHG06 show that z-coordinate simulations can indeed lead to realistic simulations at eddy-resolving resolutions. Their calculations included Laplacian viscosities in both vertical and horizontal, but no explicit diffusivity. All diapycnal mixing was therefore numerical and due to the Superbee advection scheme used. Nonetheless, at 10km resolu-

tion simulations with the Hallberg Isopycnal model compared well to the z-coordinate simulations, provided the same value of vertical viscosity was used (so that downslope descent proceeded at the same angle). The HIM simulations used a Smagorinsky horizontal viscosity parameterization, and an entrainment parameterization for diapycnal mixing [*Hallberg*, 2000]. These simulations also compare well to the POM sigma coordinate simulations of *Ezer and Mellor* [2004],*Ezer* [2005]. One key result of the LHG06 z-coordinate simulations was that diapycnal mixing was reduced at the intermediate resolutions of $\Delta x = 2.5km, \Delta z = 60m$ and $\Delta x = 10km, \Delta z = 144m$ as compared to the highest resolution simulations at $\Delta x = 500m, \Delta z = 30m$. However, in addition to changing resolution, the values of both horizontal and vertical viscosities were changed simultaneously (in order to avoid noise on the grid-scale), so the impact of changing resolution on diapycnal mixing cannot be separated from the impact of changing viscosities.

Ezer [2005] examines the impact of the Mellor-Yamada mixing scheme on the overflow simulations, using the sigma-coordinate POM at 10km horizontal resolution, by comparing the simulation with the full M-Y scheme in the vertical to two special cases in which the vertical diffusivity or vertical viscosity respectively is set identically to zero. In all 3 cases the lateral, along-sigma diffusivity has a value $100m^2/s$ with a viscosity to diffusivity ratio of 5:1. When vertical diffusivity is set to zero, diapycnal mixing is greatly reduced compared to the full Mellor-Yamada scheme, the plume descends deeper, and the plume is thinner. Setting the vertical viscosity to zero also leads to a reduction in diapycnal mixing, because the diffusivity calculated through the M-Y parameterization changes as a result of alterations in the flow caused by the viscosity. The most undiluted part of

the plume again descends deeper than for the full M-Y case, although much of the plume fluid remains near the top of the slope, due to the reduction in Ekman drainage.

Tseng and Dietrich [2006] present a series of simulations using the z-coordinate DIECAST model. In particular at a horizontal resolution of $5km$ and vertical resolution of $60m$ they vary horizontal viscosity and diffusivity and background vertical viscosity. A fourth order centered difference conservative advection scheme is used for most simulations, with much less numerical diffusion associated with it than the Superbee scheme used in LHG06, and much greater level of grid-scale noise. Vertical diffusivity and viscosity is parameterized using a *Pacanowski and Philander* [1981] Richardson number dependent scheme with a specified background vertical viscosity. (Such a scheme which is dependent on dimensional constants cannot be universally suitable for different regimes with very different velocity and length-scales). The control choice of parameters has horizontal viscosity and diffusivity set to $4m^2/s$, and background vertical viscosity set to $10^{-5}m^2/s$. Horizontal diffusivity and viscosity are changed simultaneously, and the results show little dependence on these parameters until they become large, i.e. $200m^2/s$, when the eddies are suppressed and the plume becomes more sluggish and more diluted. Changing the background vertical viscosity does not have much effect on the plume, presumably because the Richardson number dependent part of the vertical mixing dominates and is unchanged. Eliminating vertical diffusivity and viscosity altogether does have an effect, making the plume much thicker in the vertical. The authors propose that this increased thickness is due to greater vertical advection. A simulation with a second order centered difference scheme is more noisy, with less defined eddies, but largely produces similar results. When these simulations are compared with those in LHG06 the structure of the plumes more

closely resembles the highest resolution ($\Delta x = 500m$) simulations of LHG06 in that the plume does not separate from the northern boundary. This may be ascribed to the low values of vertical viscosity in TD06 (the authors state that the maximum background value of $8 \times 10^{-3} m^2/s$ is about the same as the Ri-dependent part of the viscosity whereas LHG used $5 \times 10^{-2} m^2/s$ at 2.5km resolution and $2 \times 10^{-2} m^2/s$ at 500m resolution). The tracer dilution is however more like the lower resolution LHG06 (2.5km) runs, suggesting that the use of the higher order advection scheme does not help to reduce total diffusion much compared to the Superbee scheme (presumably the explicit diffusion, both horizontal and vertical, which is necessary for stability with the less diffusive scheme is of the same order as the numerical diffusion in the Superbee scheme).

Finally, simulations of the Faroe-Bank-Channel overflow using the z-coordinate MITgcm at 2.5km resolution [*Riemenschneider and Legg*, 2007] showed a surprising dependence of mixing on the vertical viscosity. Like LHG06 no explicit diffusivity was used, so that all diffusion is attributable to the advection scheme. Large values of vertical viscosity were found to suppress vertical mixing, so that the plume was less diluted.

In summary, simulated overflow plumes show a complicated dependence on subgridscale parameterization which seems to vary from one model formulation to another. The roles of horizontal viscosity and diffusivity are difficult to distinguish since most of the studies varied the two together, but provided they are small enough not to suppress the formation of eddies, they have little effect on the model solutions. Vertical viscosities and diffusivities, being connected through complex subgridscale parameterizations in many models are even harder to separate. And finally, while the higher order scheme of Tseng and Dietrich does not seem to lead to much less mixing than the Superbee scheme used in LHG06, the

grid-scale noise it produces is highly undesirable, not just in climate simulations, but also in regional simulations where spurious tracer extrema may influence surface fluxes and biochemical models. There is therefore a need to examine advection schemes which are less diffusive than Superbee but which still prevent spurious oscillations. When diffusivity can be explicitly prescribed by a parameterization scheme (as in an isopycnal model) there is a need to examine how changing diffusivity parameterizations, independent of the model viscosity parameterization, affects the plume evolution. To this end, and to demonstrate the current state of the art in simulating overflows, here we present several new calculations carried out with the MITgcm and the Hallberg Isopycnal Model (HIM), focusing on the role of the subgridscale parameterizations in determining the simulated plume behavior.

3.1. Sensitivity of z-coordinate model simulations to viscosity and advection scheme

Here we will focus on examining the role of viscosity (both horizontal and vertical) and the advection scheme on eddy-resolving simulations of overflows. Unlike the viscosity sensitivity studies discussed above, explicit diffusivity is not simultaneously modified. We will therefore be able to ascertain the influence of viscosity on numerical mixing hinted at in *Riemenschneider and Legg* [2007]. We are not advocating the use of numerical diffusion to replace explicit diffusion parameterizations, but rather it is necessary to evaluate the level of numerical diffusion so that it can be minimized if an explicit parameterization scheme is implemented. We will examine the overall downslope transport and tracer properties of the simulated overflows at a resolution of 2.5km in the horizontal and 60m in the vertical, using the MITgcm. All have identical initial conditions and forcing: a

dense inflow is forced through the specification of boundary conditions at the entrance to a narrow channel, which then opens onto a uniform slope. The initial conditions consist of uniform stable stratification and no flow. Boundary conditions are no-slip combined with a quadratic bottom drag, as described in LHG06. These specifications correspond to "Case 1" of the DOME scenario, described in LHG06. The only differences between the calculations are in the subgridscale closures: specifically the choice of vertical and horizontal viscosities and the tracer advection schemes. All the MITgcm calculations use a Laplacian viscosity, with constant coefficients A_z and A_h in the vertical and horizontal respectively. Three different tracer advection schemes are used, applied to both buoyancy and a passive tracer. Because our intent is to examine the numerical mixing associated with the advection scheme, no explicit diffusivity is used.

Table 1 gives the values of model parameters for the different runs. We examine results for 3 different vertical viscosities and 2 different horizontal viscosities. 3 different advection schemes are examined: the Superbee flux limited advection scheme (used in LHG06); the new OS7MP advection scheme, a seventh order scheme (Adcroft, personal communication); and the Prather 2nd moment scheme [*Prather*, 1986]. The Prather advection scheme has recently been shown to greatly reduce numerical diffusion in global simulations, while both OS7MP and Prather schemes have been shown to preserve fronts while limiting diffusion in 2-dimensional tests. The calculation labeled "control" is identical to the Case 1, 2.5km resolution case described in LHG06.

In the simulations a passive tracer is injected in the inflow with a value of unity, compared to zero background value. The inflow has an initial density which matches that at the bottom of the slope. By following the evolution of the tracer field as the dense current

descends the slope we can examine the numerical mixing associated with the overflow, through both the dilution of the tracer and the migration of the tracer to lighter density classes.

Figure 1 shows the tracer just above the slope (in color) with buoyancy contours overlain, for runs with different vertical viscosities and advection schemes. The most striking result is the way in which vertical viscosity influences the simulations. Higher vertical viscosities give rise to much less dilution in both tracer and buoyancy; the almost unmixed plume descends the slope at a steep angle, with no evidence of eddies. At intermediate values of vertical viscosity eddies are visible, there is considerable mixing and the angle of descent is less steep. For the smallest vertical viscosity there is very rapid mixing, and the dilute plume moves almost along isobaths soon after entering the slope region. Vertical viscosity therefore plays a dominant role in determining the numerical mixing and the angle of descent. This result is independent of the advection scheme used: all three advection schemes show more mixing at lower vertical viscosities. The influence of advection scheme on the results is much more subtle than that of vertical viscosity. Visually there is little difference between the three runs with different advection schemes at the lowest value of vertical viscosity. For the intermediate vertical viscosity the Prather advection scheme does appear to produce slightly less dilution, and retains somewhat denser fluid in the downslope side of the plume.

The predicted lengthscale for eddies at the top of the slope $L_\rho = \sqrt{g'h_0}/f$ is about 21km, while further down the slope, g' is reduced by both mixing with ambient fluid and by approach to neutral stability level. The lengthscales of the eddies seen in the simulations are considerably larger: about 130km in diameter at the top of the slope,

while in the medium vertical viscosity simulations smaller diameter eddies are also seen lower down the slope, with diameters of about 80km. The size of the eddies at the top of the slope where they are generated does not appear to be modified by varying vertical viscosity, despite the fact that the level of mixing (and therefore g') is changed.

We can quantify the mixing by calculating the tracer-weighted buoyancy of the plume

$$\overline{b}^{\tau}(x) = \frac{\int b(x,y,z)\tau(x,y,z)dydz}{\int \tau(x,y,z)dydz} \tag{16}$$

where b is the buoyancy (relative to the surface) and τ is the tracer concentration. Figure 2a shows the weighted plume buoyancy scaled with the initial buoyancy as a function of distance from the channel entrance for all runs with the Superbee advection scheme. For the run with the highest vertical viscosity, the plume buoyancy is about 90% of its initial value, while for the lowest vertical viscosity the buoyancy is less than 50% of its initial value. Also shown are results for two runs with different horizontal viscosities - the horizontal viscosity appears to play a minor role compared to the vertical viscosity, in influencing numerical diffusion.

Figure 2b shows the weighted plume buoyancy for the intermediate vertical viscosity for the 3 different advection schemes. The OS7MP scheme generates slightly more mixing (a less dense plume), while the Prather scheme leads to slightly less mixing (a denser plume) just to the left of the inflow (at x=0). However, these differences are small when compared to the changes induced by changing vertical viscosity.

Figure 2c shows results for the lowest vertical viscosity for the 3 different advection schemes: again OS7MP leads to slightly more mixing. Now the Superbee and Prather schemes generate indistinguishable results.

To examine the role of subgridscale parameters in influencing the descent of dense fluid down the slope, we calculate the mean position of the plume (determined by the tracer distribution) as a function of along slope distance:

$$\overline{Y^{\tau}}(x) = \frac{\int y\tau(x,y,z)dydz}{\int \tau(x,y,z)dydz}. \tag{17}$$

Shown in figure 3a is the plume path for all the Superbee calculations. Higher vertical viscosity leads to a steeper descent, lower vertical viscosity leads to plumes which travel along isobaths from about 200km downstream of the inflow entrance. The Ekman numbers corresponding to the 3 different vertical viscosities are $Ek = 4 \times 10^{-5}, 10^{-2}$ and 0.1 for $A_z = 2 \times 10^{-4}, 5 \times 10^{-2}$ and $5 \times 10^{-1} m^2/s$ respectively. Note that the Ekman number for the highest vertical viscosity is close to the value at which Cenedese found a transition from eddy-dominated to laminar flow. The initial angles of descent (immediately to the left of the entrance) are $tan(\theta)$ =cross-slope distance/along-slope distance $= 0.2, 0.3$ and 0.6 respectively. These all greatly exceed the Ekman number, but more closely approach the Ekman number as viscosity increases and the Ekman drainage becomes the dominant process. At lower viscosities the Ekman drainage is only acting in a fraction of the total plume, and so ageostrophic and eddy processes dominate the initial descent. Again horizontal viscosity appears to make little difference to the results. Figure 3b and 3c show the sensitivity of plume path to advection scheme for 2 different vertical viscosities: again the differences are slight; at the intermediate viscosity the OS7MP scheme leads to a slightly less steep descent, while the Prather scheme leads to a slightly steeper descent.

One way to consider the influence of vertical viscosity is to calculate the Ekman layer thickness $\delta = \sqrt{(2A_z/f)}$ and consider how it varies relative to the total plume thickness and gridspacing. For the three values of $A_z = 2 \times 10^{-4}, 5 \times 10^{-2}$ and $5 \times 10^{-1} m^2/s$, we

have $\delta = 2, 32$, and $100m$ respectively. The actual plume thickness (as defined by the fluid with tracer concentrations of at least 10% of the inflow value) is about $450 - 1080m$, $100 - 500m$ and $210m$ respectively, with the lower viscosity cases having a large range of thicknesses due to the presence of eddies. Interestingly, as A_z is increased, the thickness of the plume is reduced, perhaps because viscous drainage is more effective at carrying fluid down the slope, or perhaps because enhanced numerical mixing is responsible for the large thicknesses in the low viscosity cases. In addition only the highest viscosity case satisfies the *Winton et al.* [1998] criteria $\delta > \alpha\Delta x$, and $\delta > \Delta z$. Hence if the Ekman layer is responsible for much of the downslope flow, this numerical configuration can only resolve that downslope flow at high values of vertical viscosity. Numerical mixing may therefore be a result of a poorly resolved Ekman layer. This would suggest that sigma-coordinate models would also be subject to the same transition in numerical mixing as a function of vertical viscosity, but would only have to satisfy the vertical constraint $\delta > D\Delta\sigma$, where D is the total depth, and $\Delta\sigma$ is the sigma-coordinate resolution.

To summarize, vertical viscosity plays a very important role in determining the behavior of a simulated dense overflow at high resolution, not just by setting the angle of descent (as would be expected) but also by modifying the numerical diffusion. This effect of vertical viscosity on numerical diffusion is independent of the advection scheme used. All three advection schemes employ limiting schemes designed to prevent grid-scale oscillations in the tracer field and it is through these limiting schemes that numerical diffusion is introduced. The vertical viscosity influences the numerical diffusion by first modifying the small-scale structure of the velocity field: smaller viscosities lead to more small-scale structure in the velocity field and require greater numerical diffusion to eliminate grid-scale

noise. Hence the smaller the vertical viscosity, the higher the numerical diffusivity and the greater the diapycnal mixing. This dependence of mixing on the vertical viscosity agrees with that observed in *Riemenschneider and Legg* [2007]. Note that *Tseng and Dietrich* [2006] see a qualitatively similar effect when their vertical viscosity parameterization is turned off: the plume appears to thicken and become more dilute.

An interesting, although discouraging, result of these simulations is that more sophisticated advection schemes do not appear to dramatically improve results at these resolutions. The Prather scheme does marginally better than the Superbee scheme, but the OS7MP scheme does worse (given that one would like to minimize numerical diffusion so that physically based parameterizations of mixing may be used instead). One cause of the OS7MP scheme's poor performance may be that the advantage of a 7th order scheme is lost when simulating a thin layer (less than 7 grid-points) close to a boundary, where the scheme behaves as a lower order scheme. A more sophisticated near-boundary formulation of the scheme could perhaps improve this result. The current implementation of the Prather scheme uses a positive-definite limiter, and a monotonicity-preserving limiter may change the Prather result (Jean-Michel Campin, private communication). For coarse resolution climate models where fronts are not resolved, the sensitivity of the behavior to advection scheme may be different than seen in these mesoscale eddy resolving simulations.

3.2. Sensitivity of isopycnal model simulations to mixing parameterization

Having discussed the dependence of numerical diapycnal mixing on advection scheme and viscosity for a z-coordinate model, we now examine the influence of explicitly parameterized mixing on the overflow simulations in a model with no numerical mixing, the

Hallberg Isopycnal Model (HIM). Three different simulations with HIM configured for the DOME scenario Case 1 are shown in figure 4. Initial conditions and forcing are as described above, one difference being that a sponge condition is used at the western and southern boundaries instead of the radiation condition used in the MITgcm calculations. Also the horizontal domain is slightly smaller (1300km rather than 1700km). All three simulations have a resolution of 2.5km in the horizontal, and 25 vertical layers with a total density difference of 2 kg/m^3. A biharmonic Smagorinsky viscosity is used in the horizontal and a constant viscosity of 1×10^{-4}m^2/s in the vertical. The three simulations are distinguished by different schemes for parameterization of the mixing between isopycnal layers. In the first simulation, there is no prescribed diapycnal mixing apart from a small background value of 1×10^{-4}m^2/s. In the second, diapycnal mixing is prescribed by the Turner scheme outlined in *Hallberg* [2000] (TP), along with the frictional boundary layer mixing described in LHG06. In the third simulation diapycnal mixing is prescribed by the new Jackson and Hallberg scheme (JH) for shear-driven mixing described in detail in *Jackson et al.* [2007], along with the frictional boundary layer mixing scheme. The tracer-weighted buoyancy and path of the plume are shown in figure 5, as defined in equations 16 and 17.

With only a small background diapycnal mixing, the plume stays close to its original density, and takes a steep path down the slope. While the steepness of the path is similar to that seen in the z-coordinate case with high vertical viscosity, there is considerable eddy behavior and plume widening in the isopycnal simulation, so that the dynamical regime is quite different, and not a laminar Ekman flow.

The two simulations with prescribed mixing look very similar, so that for these physical parameters the TP and JH schemes generate a similar amount of mixing, although the former results in slightly more mixing and a lighter plume. This similarity is despite the large difference in the critical Ri at which the turbulent mixing stops:$Ri_c = 0.8$ in TP and $Ri_c = 0.25$ in JH. (It should be noted however that when the same parameterization schemes are used in the equatorial regions, with no change in parameters, the JH scheme produces much less mixing than TP, and therefore performs much better.) Like the z-coordinate simulations, most of the mixing occurs just after the plume enters the slope region, and the plume forms a series of large eddies through instability, however with the mixing parameterization schemes there is also some mixing and a decrease in buoyancy along the slope as seen in Figure 5a. The solutions in Figure 4 for both the JH and TP mixing schemes are qualitatively most similar to the z-coordinate cases with intermediate vertical viscosity in Figure 1b,d,f: the plume is not as dilute as in the low viscosity cases and, although it is mainly flowing along isobaths it shows some signs of separating from the wall and proceeding downslope (Figure 5b) as in the intermediate viscosity case. Both the final buoyancy of the plume and the angle of descent are in between those of the z-coordinate cases with intermediate and low vertical viscosity. The vertical viscosity in the isopycnal model is close to that in the low vertical viscosity case z-coordinate simulation, so that at this value of vertical viscosity the mixing induced by the numerical scheme in the z-coordinate model exceeds the mixing due to the parameterization scheme in the isopycnal model.

Given that the parameters in the JH diffusivity parameterization have been chosen carefully with reference to direct numerical simulation, this simulation might be regarded

as our best estimate of the actual amount of mixing one would expect in this physical scenario, in the absence of definitive laboratory measurements of mixing. A z-coordinate scheme without an explicit mixing parameterization gives more mixing for a similar vertical viscosity, hence until the numerical mixing can be reduced in the z-coordinate simulation, there is little point in focusing attention on implementing sophisticated schemes to parameterize the mixing in such a model. One way to reduce the mixing below the level of parameterized mixing in the isopycnal model is to increase the vertical viscosity; however this also suppresses eddy behavior and the simulated plume is then governed entirely by Ekman dynamics.

4. Discussion and conclusions

Mesoscale eddies are a feature of many overflows. These eddies may be generated by either barotropic instability when overlying water is transported to deeper depth during the geostrophic adjustment process, or by baroclinic instability of the geostrophically adjusted dense fluid on the slope. (In fact, examination of the vorticity field in the simulations described above suggests that both processes may operate within the same overflow - largely barotropic cyclonic vortices are found in the upper layers, close to the coast, generated through barotropic instability, while the dense water below is carried further downslope by more baroclinic eddies.) We have reviewed the literature regarding the formation of eddies in overflows and shown that eddies exist when rotation plays an important role in the overflow dynamics, so that the overflow comes under the influence of rotation before it reaches its neutral buoyancy level, or the bottom of the slope. If frictional effects are large, so that the thickness of the overflow plume is close to the Ekman layer thickness, then the plume forms a laminar Ekman layer and eddies are

suppressed. Similarly, if Froude numbers are large, the supercritical flow does not form eddies until a transition is made to a subcritical regime.

While mesoscale eddies are easily captured by high resolution ocean models, the much smaller-scale eddies responsible for overturning and mixing cannot be resolved. The diapycnal mixing they are responsible for therefore remains the most significant challenge for overflow simulations, and plays a dominant role in determining the dilution of overflow water, setting the tracer properties and volume of the final product water mass. Models are forced to represent this diapycnal mixing through diffusivity parameterizations. Unfortunately diapycnal mixing also results from numerical diffusion in level coordinate and sigma-coordinate models, complicating matters. We have therefore critically examined the diapycnal mixing in mesoscale-eddy resolving overflow simulations, and examined its dependence on both explicit diffusivity parameterizations and on model numerics. Many past studies are complicated because viscosity and diffusivity are varied simultaneously and little attempt is made to quantify numerical diffusion. Ideally, one would like a model with negligible numerical diffusion in which all diapycnal mixing is prescribed through an explicit parameterization. To that end it is necessary to identify model configurations with the minimum numerical diffusion. To complement earlier studies we have therefore described several new simulations focusing on the numerical diffusion in a z-coordinate model (the MITgcm) and its sensitivity to model viscosity and advection scheme, and on the influence of diapycnal mixing parameterization in an isopycnal-coordinate model. Numerical diffusion in a z-coordinate model was found to depend strongly, in an inverse sense, on vertical viscosity, since the advection scheme introduces sufficient numerical diffusion to remove any grid scale noise caused by low values of vertical viscosity. We strongly

suspect that a similar dependence would be found in a sigma-coordinate model. Since all the numerical diffusion is a result of the advection scheme, we examined the sensitivity to advection scheme, and found that while the Prather advection scheme performed a little better than the others, in terms of reducing numerical diffusion, the difference was not large. Finally, while the presence of a diapycnal mixing scheme was found to strongly influence the isopycnal model simulations, the exact nature of that scheme was not found to have a strong influence for this physical scenario (given that parameters have been chosen appropriately in both schemes).

Mesoscale-eddy-resolving models of overflows therefore have to make many choices in order to correctly capture both the resolved physics and the unresolved diapycnal mixing. These include the vertical coordinate, the advection scheme, and the viscosity and diffusivity parameterization. If sigma-coordinate or z-coordinate models are used, they will inherently have numerical diffusion, and the least diffusive advection scheme would be preferable. However, there is little point choosing a non-diffusive scheme if that scheme generates so much noise as to require large values of explicit diffusivity. The horizontal viscosity should obviously be small enough to permit eddies, but otherwise this choice is not too important. The vertical viscosity however does play an important role. For a constant vertical viscosity it seems appropriate, in order to prevent too much mixing, to choose a value as large as possible without forcing the plume into the large Ekman number laminar regime. For a variable eddy viscosity parameterization (e.g. Mellor-Yamada) further studies are needed to understand the overflow mixing resulting from the M-Y scheme and how it compares with constant vertical viscosity simulations. Given the complex spatial distribution of vertical viscosity in the gravity current when using the M-Y scheme

(e.g. figure 3 in *Ezer* [2005]), it is unclear if the large sensitivity to viscosity found here will apply to variable eddy viscosity cases.

Isopycnal simulations have the advantage that the advection scheme does not cause diapycnal mixing, and that the amount of mixing can be directly controlled by the mixing parameterization, completely independently of the vertical viscosity (which also influences the plume path and the eddy dynamics).

Acknowledgments. This paper is a contribution of the Gravity Current Entrainment Climate Process Team, funded by NSF and NOAA as part of USCLIVAR, and we would like to thank other team members for sharing their results. We would also like to thank the ocean model development teams at MIT (especially Jean-Michel Campin) and at GFDL (especially Alistair Adcroft), for allowing us to test their recently implemented advection schemes in the overflow configuration. Comments from Anand Gnanadesikan, Matthew Harrison and two anonymous reviews helped to improve the manuscript. We also thank Mathew Hecht and Hiro Hasumi for inviting us to contribute this chapter.

References

Bruce, J., Eddies southwest of the denmark strait, *Deep Sea Res.*, *42*, 13–29, 1995.

Cenedese, C., J. A. Whitehead, T. Ascarelli, and M. Ohiwa, A Dense Current Flowing down a Sloping Botton in a Rotating Fluid, *J. Phys. Oceanogr.*, *34*, 188–203, 2004.

Chang, Y. S., T. Özgökmen, H. Peters, and X. Xu, Numerical simulation of the Red Sea outflow using HYCOM and comparison with REDSOX observations, *J. Phys. Oceanogr.*, *in press*, 2007.

Decamp, S., and J. Sommeria, Scaling properties for turbulent gravity currents deviated by Coriolis effect on a uniform slope, *J. Fluid. Mech.*, *submitted*, 2007.

Ellison, T., and J. Turner, Turbulent entrainment in stratified flows, *J. Fluid. Mech.*, *6*, 423–448, 1959.

Etling, D., F. Gelhardt, U. Schrader, F. Brennecke, G. Kuhn, G. C. d'Hieres, and H. Didelle, Experiments with density currents on a sloping bottom in a rotating fluid, *Dynamics of Atmospheres and Oceans*, *31*, 139–164, 2000.

Ezer, T., Entrainment and diapycnal mixing in three-dimensional bottom gravity simulations using the Mellor-Yamada turbulence scheme, *Ocean Modelling*, *9*, 151–168, 2005.

Ezer, T., Topographic influence on overflow dynamics: idealized numerical simulations and the Faroe Bank Channel overflow, *J. Geophys. Res.*, *111*, doi:1029/2005JC003,195, 2006.

Ezer, T., and G. Mellor, A generalized coordinate ocean model and a comparison of the bottom boundary layer dynamics in terrain-following and z-level grids, *Ocean Modelling*, *6*, 379–403, 2004.

Geyer, F., S. Osterhus, B. Hansen, and D. Quadfasel, Observations of highly regular oscillations in the overflow plume downstream of the Faroe Bank Channel, *J. Geophys. Res.*, *111*, C12,020, 2006.

Girton, J., L. J. Pratt, D. Sutherland, and J. Price, Is the Faroe Bank Channel overflow hydraulically controlled?, *J. Phys. Oceanogr.*, *36*, 2340–2349, 2006.

Gordon, A., E. Zambianchi, A. Orsi, M. Visbeck, C. Giulivi, T. Whitworth, and G. Spezie, Energetic plumes over the western Ross Rea continental slope, *Geophys. Res. Lett.*, *31*, L21,302, 2004.

Hallberg, R., Time Integration of Diapycnal Diffusion and Richardson Number - Dependent Mixing in Isopycnal Coordinate Ocean Models, *Mon. Wea. Rev.*, *128*, 1402–1419, 2000.

Holland, D., R. Rosales, D. Stephanica, and E. Tabak, Internal hydraulic jumps and mixing in two-layer flows, *J. Fluid. Mech.*, *470*, 63–83, 2002.

Jackson, L., R. Hallberg, and S. Legg, A parameterization of shear-driven turbulence for ocean climate models, *J. Phys. Oceanogr.*, *submitted*, 2007.

Jiang, L., and R. Garwood, Three-dimensional Simulations of Overflows on Continental Slopes, *J. Phys. Oceanogr.*, *26*, 1214–1233, 1996.

Jiang, L., and R. Garwood, Effects of topographic steering and ambient stratification on overflows on continental slopes: A model study, *J. Geophys. Res.*, *103*, 5459–5476, 1998.

Jungclaus, J., and G. Mellor, A three-dimensional model study of the Mediterranean outflow, *J. Mar. Sci.*, *24*, 41–66, 2000.

Kase, R., and A. Oschlies, Flow through Denmark Strait, *J. Geophys. Res.*, *105*, 28,527–28,546, 2000.

Käse, R., J. Girton, and T. Sanford, Structure and variability of the Denmark Strait Overflow: model and observations, *J. Geophys. Res.*, *108*, doi:10.1029/2002JC001,548, 2003.

Kida, S., Overflows and upper ocean interaction: a mechanism for the Azores current, Ph.D. thesis, MIT-WHOI Joint program in oceanography, 2006.

Kida, S., J. Price, and J. Yang, The upper oceanic response to overflows: a mechanism for the Azores Current, *J. Phys. Oceanogr.*, *submitted*, 2007.

Killworth, P., On th erate of descent of overflows, *J. Geophys. Res.*, *106*, 22,267–22,275, 2001.

Lane-Serff, G., and P. Baines, Eddy formation by dense flows on slopes in a rotating fluid, *J. Fluid. Mech.*, *363*, 229–252, 1998.

Lane-Serff, G., and P. Baines, Eddy Formation by Overflows in Stratified Water, *J. Phys. Oceanogr.*, *30*, 327–337, 2000.

Legg, S., R. Hallberg, and J. Girton, Comparison of entrainment in overflows simulated by z-coordinate, isopycnal and nonhydrostatic models, *Ocean Modelling*, *11*, 69–97, 2006.

Mauritzen, C., J. Price, T. Sanford, and D. Torres, Circulation and mixing in the Faroese Channels, *Deep Sea Res.*, *52*, 883–913, 2005.

Mellor, G., and T. Yamada, Development of a turbulent closure model for geophysical fluid problems, *Reviews of Geophysics*, *20*, 851–875, 1982.

Mellor, G., S. Hakkinen, T. Ezer, and R. Patchen, A generalization of a sigma coordinate ocean model and an intercomparison of model vertical grids., *Ocean Forecasting: Conceptual basis and applications, N. pinardi and J. D. Woods (Eds.).*

Nof, D., The translation of isolated cold eddies on a sloping bottom, *Deep Sea Res.*, *30*, 171–182, 1983.

Özgökmen, T., and E. Chassignet, Dynamics of two-dimensional turbulent bottom gravity currents, *J. Phys. Oceanogr.*, *32*, 1460–1478, 2002.

Pacanowski, R., and S. Philander, Parameterization of vertical mixing in numerical models of tropical ocean, *J. Phys. Oceanogr.*, *11*, 1443–1451, 1981.

Papadakis, M., E. Chassignet, and R. Hallberg, Numerical simulations of the Mediterranean sea outflow: impact of the entrainment parameterization in an isopycnic coor-

dinate ocean model, *Ocean Modelling*, *5*, 325–356, 2003.

Peters, H., and W. Johns, Bottom layer turbulence in the Red Sea outflow plume, *J. Phys. Oceanogr.*, *36*, 1763–1785, 2006.

Peters, H., W. Johns, A. Bower, and D. Fratantoni, Mixing and entrainment in the Red Sea Outflow Plume. Part I. Plume Structure, *J. Phys. Oceanogr.*, *35*, 569–583, 2005.

Pickart, R. S., D. J. Torres, and P. S. Fratantoni, The East Greenland Spill Jet, *J. Phys. Oceanogr.*, *35*, 1037Ž2013–1053, 2005.

Prather, M., Numerical advection by conservation of second-order moments, *J. Geophys. Res.*, *91*, 6671–6681, 1986.

Pratt, L., U. Riemenschneider, and K. Helfrich, A transverse hydraulic jump in a model of the Faroe Bank Channel outflow, *Ocean Modelling*, *in press*, 2007.

Price, J., and M. Baringer, Overflows and deep water production by marginal seas, *Progress in Oceanography*, *33*, 161–200, 1994.

Price, J., M. Baringer, R. Lueck, G. Johnson, L. Ambar, G. Parrilla, A. Cantos, M. Kennelly, and T. Sanford, Mediterranean outflow mixing and dynamics, *Science*, *259*, 1277–1282, 1993.

Riemenschneider, U., and S. Legg, Regional simulations of the Faroe Bank Channel overflow in a level model, *Ocean Modelling*, *17*, 93–122, 2007.

Serra, N., and I. Ambar, Eddy generation in the Mediterranean Undercurrent, *Deep Sea Res. II*, *49*, 4225–4243, 2002.

Smith, P., Experiments with viscous source flows in rotating systems, *Dynamics of Atmospheres and Oceans*, *1*, 241–272, 1977.

Spall, M., and J. Price, Mesoscale variability in Denmark Strait: the PV outflow hypothesis, *J. Phys. Oceanogr.*, *28*, 1598–1623, 1998.

Swaters, G., On the baroclinic instability of cold-core coupled density fronts on a sloping continental shelf, *J. Fluid. Mech.*, *224*, 361–382, 1991.

Tseng, Y.-H., and D. Dietrich, Entrainment and transport in idealized three-dimensional gravity current simulation, *J. Ocean. Atmos. Tech.*, *23*, 1249–1269, 2006.

Winton, M., R. Hallberg, and A. Gnanadesikan, Simulation of Density-Driven Frictional Downslope Flow in Z-Coordinate Ocean Models, *J. Phys. Oceanogr.*, *28*, 2163–2174, 1998.

Xu, X., E. Chassignet, J. Price, T. Özgökmen, and H. Peters, Numerical representation of the Mediterranean outflow in the Gulf of Cadiz, *J. Geophys. Res.*, *submitted*, 2007.

Simulation	$A_z(m^2/s)$	$A_h(m^2/s)$	Advection scheme
Control	5×10^{-2}	5.0	Superbee
Low A_z	2×10^{-4}	5.0	Superbee
High A_z	5×10^{-1}	5.0	Superbee
Low A_h	5×10^{-2}	0.5	Superbee
High A_h	5×10^{-2}	50	Superbee
OS7MP Med A_z	5×10^{-2}	5.0	OS7MP
OS7MP Low A_z	2×10^{-4}	5.0	OS7MP
Prather Med A_z	5×10^{-2}	5.0	Prather
Prather Low A_z	2×10^{-4}	5.0	Prather

Table 1. Values of model parameters in the MITgcm simulations

(a) $A_z = 5 \times 10^{-1} m^2/s$, Superbee

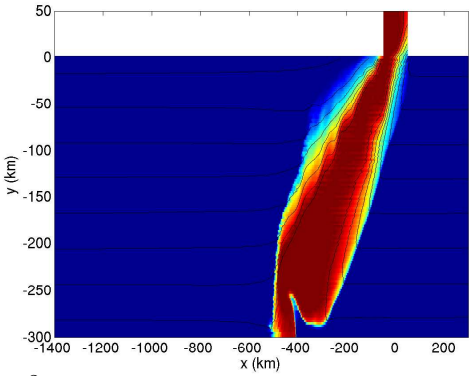

(b) $A_z = 5 \times 10^{-2} m^2/s$, Superbee

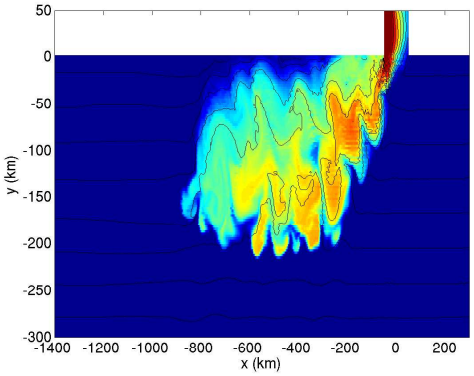

(c) $A_z = 2 \times 10^{-4} m^2/s$, Superbee

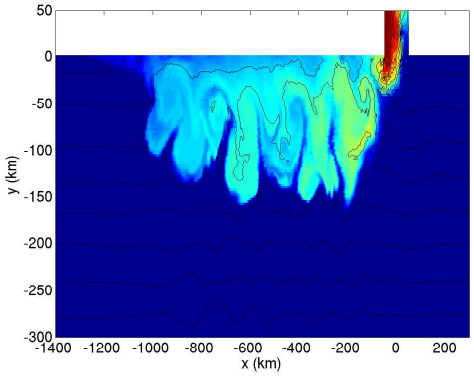

(d) $A_z = 5 \times 10^{-2} m^2/s$, OS7MP

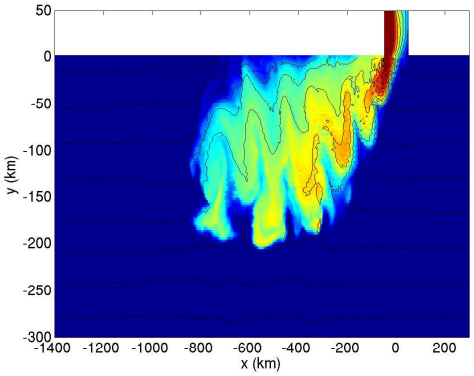

(e) $A_z = 2 \times 10^{-4} m^2/s$, OS7MP

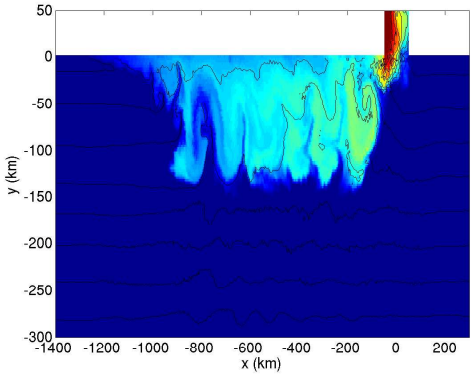

(f) $A_z = 5 \times 10^{-2} m^2/s$, Prather

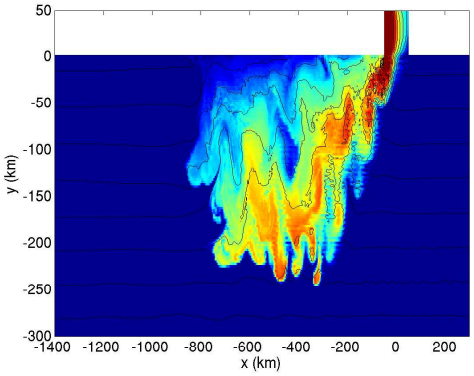

(g) $A_z = 2 \times 10^{-4} m^2/s$, Prather

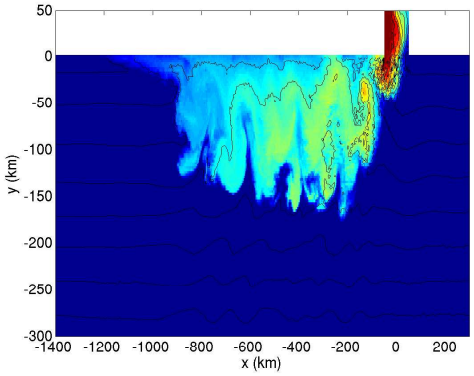

Figure 1. Snapshots of the passive tracer field just above the topography (in color) with buoyancy contours overlain. Passive tracer has an initial value of zero in the ambient fluid, and is set to 1 in the inflow. Mixing between inflow water and ambient fluid causes dilution

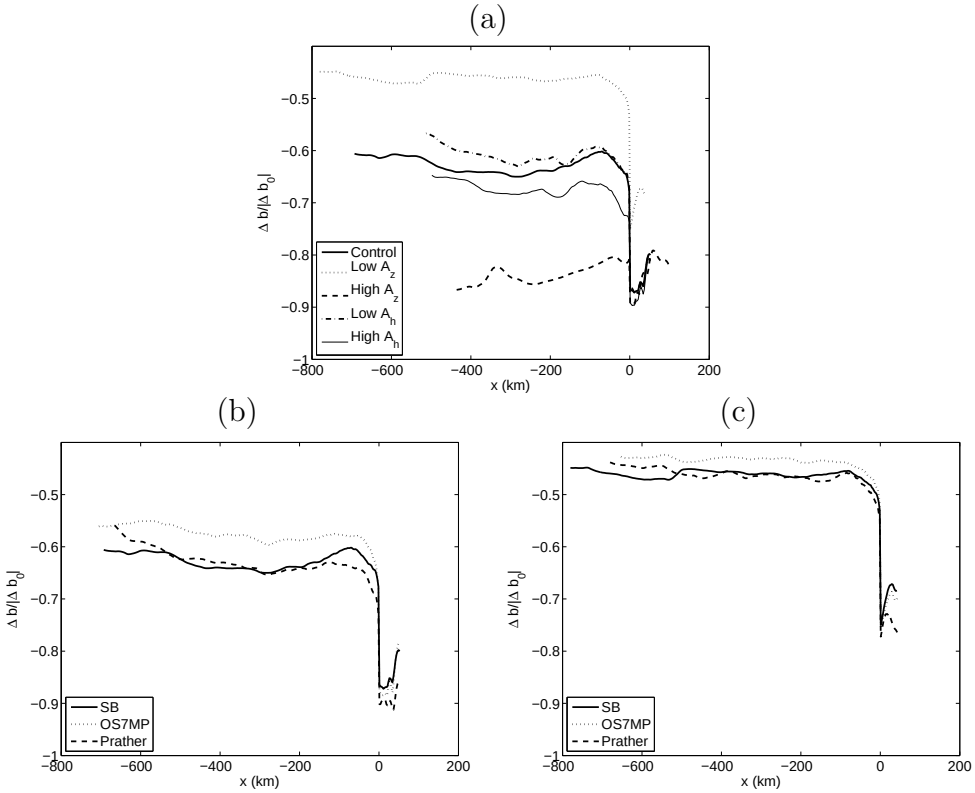

Figure 2. The tracer-weighted plume buoyancy, as a function of along-slope distance from the channel entrance, for the MITgcm calculations. (a) All simulations with the Superbee advection scheme, with different horizontal and vertical viscosities. (b) Simulations with $A_z = 5 \times 10^{-2} m^2/s$, with different advection schemes. (c) Simulations with $A_z = 2 \times 10^{-4} m^2/s$, with different advection schemes.

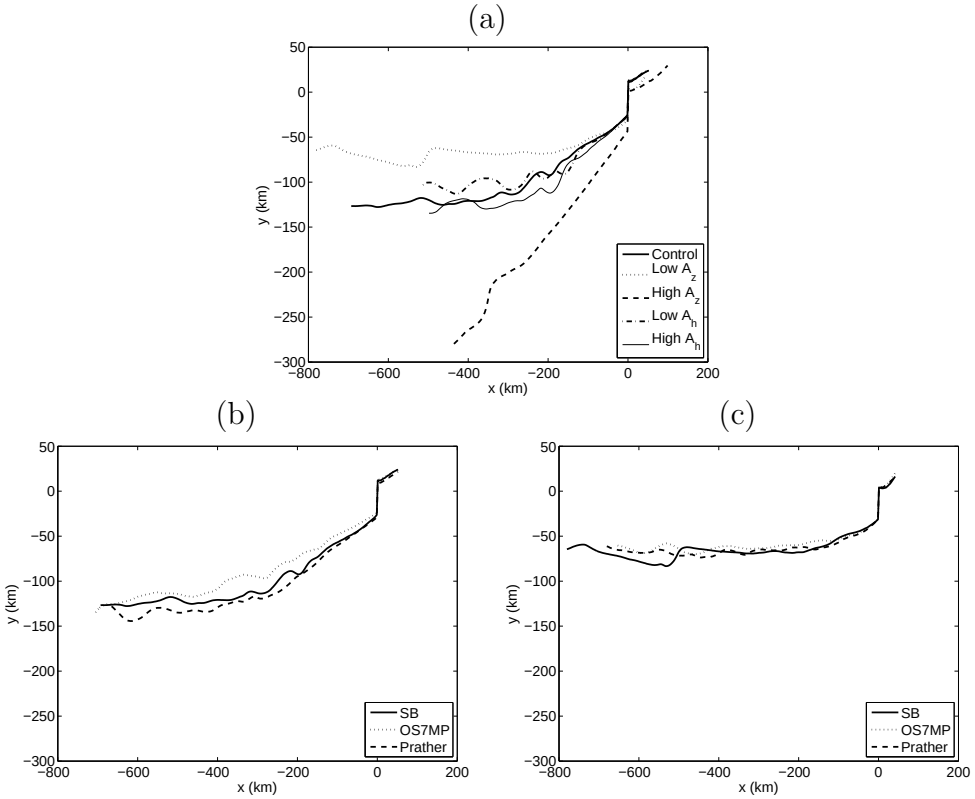

Figure 3. The tracer-weighted plume path for the MITgcm calculations. (a) All simulations with the Superbee advection scheme, with different horizontal and vertical viscosities. (b) Simulations with $A_z = 5 \times 10^{-2} m^2/s$, with different advection schemes. (c) Simulations with $A_z = 2 \times 10^{-4} m^2/s$, with different advection schemes.

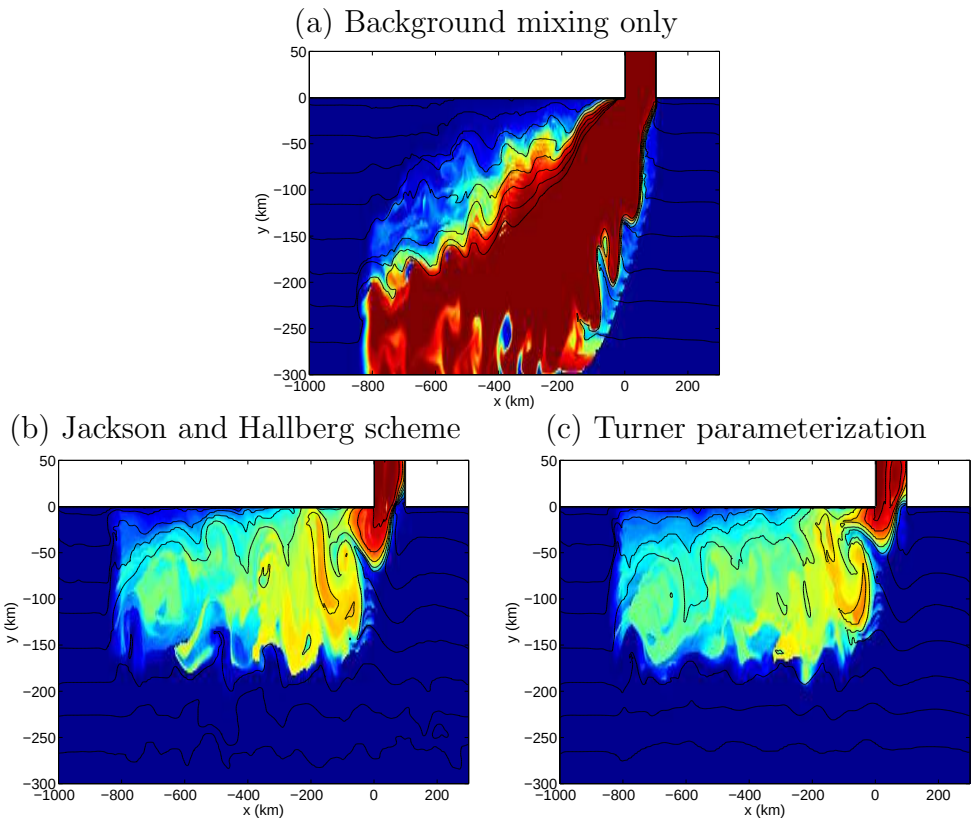

Figure 4. Snapshots of the passive tracer field just above topography (in color) with buoyancy contours overlain. The snapshots are for a time 40 days after the beginning of the simulation. All calculations are carried out with the Hallberg Isopycnal Model with different parameterizations of diapycnal mixing.

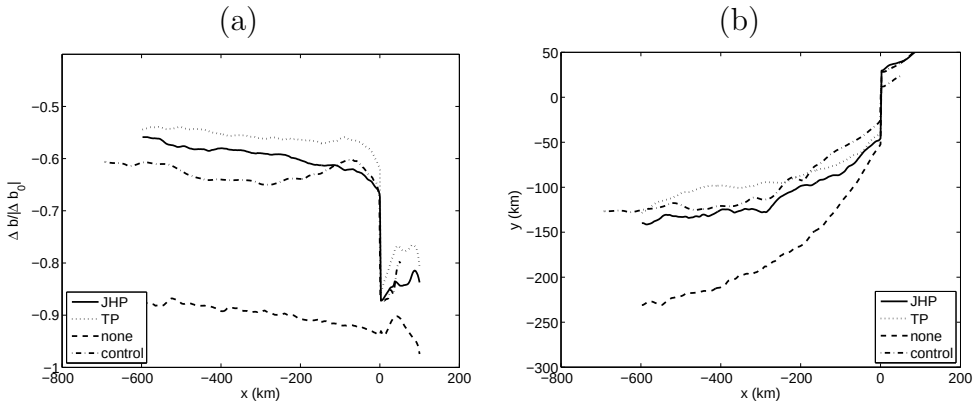

Figure 5. For the Hallberg Isopycnal Model simulations: (a) the tracer-weighted plume buoyancy, as a function of along-slope distance from the channel entrance; (b) the tracer-weighted plume path. Results are shown for three different diapycnal mixing parameterizations: "no mixing" (i.e. only weak background mixing), Jackson-Hallberg scheme (JHS) and Turner Parameterization (TP). For comparison, the MITgcm control simulation is also shown.